

Microparticle-based Controlled Drug Delivery Systems: From Experiments to Statistical Analysis and Design

Sebastian Lotter^{*}, Tom Bellmann[†], Sophie Marx[†], Mara Wesinger[†], Lukas Brand^{*},
Maximilian Schäfer^{*}, Dagmar Fischer[†], and Robert Schober^{*}

^{*}Institute for Digital Communications, Friedrich-Alexander-Universität Erlangen-Nürnberg (FAU), Erlangen, Germany

[†]Division of Pharmaceutical Technology and Biopharmacy, FAU, Erlangen, Germany

Abstract—Controlled drug delivery (CDD), the controlled release and delivery of therapeutic drugs inside the human body, is a promising approach to increase the efficacy of drug administration and reduce harmful side effects to the body. CDD has been a major research focus in the field of molecular communications (MC) with the goal to aid the design and optimization of CDD systems with communication theoretical analysis. However, the existing studies of CDD under the MC framework are purely theoretical, and the potential of MC for the development of practical CDD applications remains yet to be shown. This paper presents a step towards filling this research gap. Specifically, we present a novel MC-based model for a specific CDD system in which drugs are embedded into microparticles and released gradually towards the target site. It is demonstrated that the proposed model is able to faithfully reproduce experimental data. Furthermore, statistical analysis is conducted to explore the impact of the microparticle size on the drug release. The presented results reveal the sensitivity of the drug release to changes in the microparticle size. In this way, the proposed model can be used for the design of future microparticle-based CDD systems.

I. INTRODUCTION

Molecular communications (MC) denotes a recently emerging communication paradigm that considers the transmission of information by means of chemical information carriers. Specifically and in contrast to conventional communication based on electromagnetic waves, *molecules* are used to transmit information in MC. The inspiration for MC hereby stems from natural MC systems, in which biological entities like cells and organs encode and exchange information using molecules. MC is the endeavour to leverage this natural form of communication for in-body applications that require synthetic communication [1].

One important example application in this context is *controlled drug delivery (CDD)*. In CDD, therapeutic drugs shall be deployed to a target site inside the human body such that side effects on the rest of the body are minimized. Under the conceptual framework of MC, the CDD scenario resembles a communication system where an engineered transmitter (Tx), the drug releasing device, emits a signal, the drug molecules, that propagates over a physical channel, e.g., the cardiovascular system, towards the receiver (Rx), i.e., the target site. The Rx in such systems are typically predetermined by the specific application. Accordingly, the communication engineering challenge in developing CDD systems resides mainly in the Tx design.

In this paper, we focus on one specific CDD system, in which drug molecules are delivered in a controlled manner from a wound dressing on the human skin to the wound. The challenge in designing such systems is to guarantee a particular drug supply rate to the wound during the time the wound dressing is applied. The specific system under consideration is a wound dressing containing drug-loaded polymer microparticles. In this system, drug release occurs in a two-step process. In a first step, drug molecules are released from the microparticles into the aqueous matrix of the wound dressing itself. Then, in the second step, the drug molecules migrate from the wound dressing into the wound. There are several tunable parameters in this system, such as the size of the microparticles, which can be exploited to realize a specific drug supply rate at the target site, i.e., the wound. In order to understand the possibilities and limits of the considered system in terms of the achievable drug release profiles, mathematical modeling, specifically under the MC framework, can be a natural and valuable tool.

CDD has been a focus of MC research for more than ten years and early progress in applying MC in the context of CDD has been summarized in several survey papers [2], [3]. Most of the recent works on CDD in MC focus on the development of communication theoretical models to aid the design of efficient drug delivery systems [4], [5]. Besides, there are some works that consider the physics-based modeling of specific MC system components such as the Tx [6], [7]. Most MC-based CDD models are *bottom-up* models, i.e., starting from a set of assumptions about its components, the behavior of the entire system is derived in an *inductive* manner. The power of this approach lies in the fact that the impact of physically meaningful system parameters, such as particle sizes or reaction rate constants, is reflected in the model. The drawback, however, is that bottom-up models either rely on highly idealized assumptions regarding the considered system, e.g., with respect to the relevant chemical processes, or entail high-dimensional parameter spaces. In both cases it is difficult or even impossible to validate the models using experimental data and, consequently, their relevance for practical system design remains yet to be shown.

On the other hand, drug release models derived by experimentalists follow a different philosophy. Here, mostly *top-down* models are considered and *deductive* reasoning is applied. For example, a popular top-down model to describe

experimentally observed drug release from microparticles is the so-called *Ritger-Peppas* model. In this model, the relative drug release is modeled as

$$\frac{M_t}{M_\infty} = kt^n, \quad (1)$$

where M_t/M_∞ denotes the relative amount of released drug at time t , and $k > 0$ and $n > 0$ are fitting parameters. Based on the value of n obtained from parameter fitting to experimental data, the dominant release kinetics can be *deduced*, e.g., $n \approx 1/2$ would correspond to diffusion-dominated drug release [8]. The drawback of (1) and other top-down models (see [9] for a review) is that they are not well-suited for system design, since they do not reflect changes in the values of the physical system parameters.

In this paper, we propose, validate, and study a novel MC-based model for the CDD from microparticles embedded into a specific type of wound dressing. In contrast to existing models, the proposed model integrates both *descriptive* and *normative* features. In particular, we demonstrate that the model is capable of faithfully reproducing experimental data, achieving higher accuracy than benchmark top-down models with the same number of fitting parameters. Furthermore, we present a statistical analysis that shows how the proposed model can be exploited to deduce insights for system design. The presented results specifically provide novel insights on the role that the microparticle size can play in tailoring and optimizing the considered CDD system.

The remainder of the paper is organized as follows. In Section II, the considered experimental CDD setup and the analytical system model are introduced. Section III presents the statistical analysis of the proposed model. In Section IV, numerical results are presented, and Section V concludes the paper with a brief summary and an outlook towards future research directions.

II. SYSTEM MODEL

A. Experimental Setup

In the CDD system under consideration, drug molecules shall be released in a controlled manner from a wound dressing to the wound. When realized and applied in practice, such CDD systems can, for example, enable the anti-microbial treatment of a burn wound during the healing process [10]. Specifically, we consider the release of *cannabidiol* (CBD), a highly lipophilic drug, from a *bacterial nanocellulose* (BNC) fleece. BNC is a biological material produced by bacteria [11] and BNC fleeces are ideally suited as wound dressings due to their high water content, biocompatibility, biodegradability, and thermal and mechanical stability. To integrate the lipophilic CBD molecules into the aqueous environment inside the BNC fleece, they are encapsulated into degradable microparticles synthesized from *poly(lactic-co-glycolic acid)* (PLGA) polymers, i.e., carboxylic acid-based biopolymers [12, Ch. 7]. The PLGA-based microparticles (PMP) are synthesized *in situ* [13], i.e., inside the BNC fleece, and hence may be subject to different synthesis conditions depending on the microstructure of the respective BNC fleece.

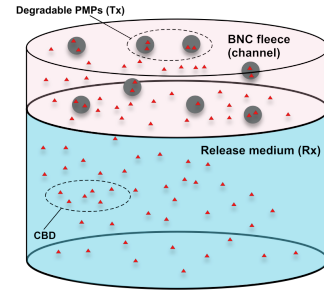


Fig. 1. Schematic illustration of the considered experimental setup. Drug molecules (red triangles) are released from degradable microparticles (grey disks) into the wound dressing (top part of the cylinder) before they migrate into the release medium (bottom part of the cylinder).

Fig. 1 illustrates the considered CDD system schematically. In the experiment, the BNC fleece containing the CBD-loaded PMPs is placed on top of a release medium. After the PMPs start to degrade, CBD molecules are released into the BNC fleece from which they further migrate into the release medium. The release medium is sampled by the experimenter at predefined time instants to determine the CBD release profile over time.

A complete specification of the considered experimental setup is presented in [13]. From this specification, the following conclusions relevant for the further modeling can be drawn.

- 1) Both the release of CBD from the PMPs into the BNC and from the BNC into the release medium are driven by the corresponding concentration gradients.
- 2) The BNC fleece and the release medium can be considered perfect sinks, i.e., the migration of CBD molecules in reverse direction is negligible for both release processes.
- 3) There is no diffusion barrier to be considered between the BNC fleece and the release medium.
- 4) The PMPs are uniformly distributed inside the BNC matrix and the release medium is well-stirred.

The PMPs are biodegradable and start to erode upon contact with the aqueous medium inside the BNC fleece. Interestingly, manipulating this process by adjusting the properties of the PMPs, e.g., their sizes, presents a degree of freedom by which the drug release can be controlled. The results presented later in this paper provide quantitative insights into how this can be achieved.

B. MC System Model

In this section, we match the components of the CDD system described in the previous section to communication system components and provide mathematical models for each of the components. In this way, an MC-based end-to-end model of the CBD release is obtained.

1) *Transmitter*: Within the MC framework, the PMPs and the (normalized) amount of CBD released from the PMPs into the BNC fleece per unit time, denoted in the following as $x(t)$, correspond to the Tx and the transmit signal, respectively. Several studies [14]–[16] have accumulated experimental evidence that drug release from PMPs can be modelled as a diffusion process. Hence, $x(t)$ is obtained as the solution to the

spherical diffusion equation with Dirichlet boundary condition and uniform initial concentration as follows¹ [14], [17]

$$x(t) = \frac{6D_i}{R_i^2} \sum_{n=1}^{\infty} \exp\left(-\frac{D_i n^2 \pi^2}{R_i^2} t\right), \quad t \geq 0, \quad (2)$$

where R_i and D_i denote the radius of the PMPs in mm and the *effective* diffusion coefficient in $\text{mm}^2 \text{h}^{-1}$ of the CBD molecules inside the PMPs, respectively.

It is important to note that the “diffusion” in this context does not exclusively arise from Brownian motion inside the PMPs. Instead, it results from several bio-physical processes including Brownian motion, but also other effects such as (electro-)chemical interactions of the drug molecules with the porous PMP matrix and the medium. In fact, it has been observed that the porous inner structure of the PMPs depends on R_i [14]. Since D_i models the effective mobility of the drug molecules inside this structure, the two model parameters R_i and D_i are, hence, correlated. To incorporate this effect into (2), an exponential model of the following form has been proposed in [14]

$$D_i = \hat{D}_i R^\omega, \quad (3)$$

where \hat{D}_i in $\text{mm}^2 \text{h}^{-1}$ and $R = R_i/(1 \text{ mm})$ denote a scaling constant independent of the particle radius and the dimensionless normalized particle radius, respectively, and $\omega \geq 0$ indicates the degree to which R_i and D_i are correlated.

Substituting (3) in (2), we obtain

$$x(t) = \frac{6}{\pi^2} \sum_{n=1}^{\infty} \frac{\tilde{D}_i \alpha_n^2}{n^2} \exp\left(-\tilde{D}_i \alpha_n^2 t\right), \quad (4)$$

where $\tilde{D}_i = \hat{D}_i/1 \text{ mm}^2$ and $\alpha_n = n\pi/R^{1-\omega/2}$.

The value of ω is highly drug-specific, depending for example on the electrostatic interactions between the specific drug molecules and the PMP polymers [15]. However, since $\omega > 2$ would correspond to a positive correlation between $x(t)$ and R in (4), contradicting experimental observations [15], we restrict our considerations to $\omega \in [0, 2)$.

From (4), we observe that $x(t)$ is relatively sensitive with respect to changes in R for values of ω close to 0 and relatively insensitive for values of ω close to 2. Hence, the value of ω in (3) determines whether R can be a suitable design parameter for the considered CDD system. In Section IV, we study the impact of ω on the sensitivity of the end-to-end drug release to changes in R in a quantitative manner.

2) *Channel*: According to Section II-A, the drug molecules released from the PMPs propagate inside the BNC fleece towards the release medium. Hence, in the MC framework, the BNC fleece corresponds to the channel.

Since the BNC fleece essentially behaves like a fluid medium (the water content is $> 90\%$ [11]), it is reasonable to assume that the CBD propagation exhibits diffusion dynamics. In line with this assumption, diffusion-controlled drug release from BNC has also been reported in [18]. Now, since (i) drug molecules can leave the BNC fleece only at its interface with the release medium, (ii) PMPs are uniformly distributed

inside the BNC patch, and (iii) the diffusive resistance at the interface layer is negligible as compared to the diffusive resistance inside the fleece [13], the channel impulse response, denoted by $h(t)$, is obtained by solving the one-dimensional diffusion equation for a closed interval with one Neumann (upper boundary of the fleece in Fig. 1) and one Dirichlet boundary (interface of BNC fleece with release medium) and uniform initial condition as follows [17, Eq. (4.18)]

$$h(t) = \frac{8}{\pi^2} \sum_{m=1}^{\infty} \frac{D_o \beta_m}{(2m-1)^2} \exp(-D_o \beta_m^2 t), \quad t \geq 0, \quad (5)$$

where D_o denotes the diffusion coefficient of the CBD inside the BNC fleece, but outside the PMPs, in $\text{mm}^2 \text{h}^{-1}$ and $\beta_m = (2m-1)\pi/(2a)$, with a denoting the height of the BNC fleece in mm.

Eq. (5) has been previously used to describe the drug release from a drug carrier film, e.g., in [15]. For the system considered in this paper, we verify in Section IV with experimental data that (5) is indeed a suitable channel model.

3) *Receiver*: The physical Rx in the considered CDD system is the release medium, cf. Section II-A. Conceptually, the Rx is a transparent, molecule counting Rx, i.e., it counts the cumulative amount of CBD released into the release medium by time t and does otherwise not interact with the drug molecules. Since the considered system can be assumed to be linear and time-invariant, cf. Section II-A, the *expected received signal*, $r(t)$, is obtained as $r(t) = \int_0^t x(\tau) * h(\tau) d\tau$, where $*$ denotes the convolution operator. Substituting (2) and (5), we obtain after straightforward integration

$$r(t) = 1 - \frac{6}{\pi^2} \sum_{n=1}^{\infty} \left[\frac{1}{n^2} \exp\left(-\frac{\tilde{D}_i n^2 \pi^2}{R^{2-\omega}} t\right) - \sum_{m=1}^{\infty} \frac{1}{(2m-1)^2} \frac{8\tilde{D}_i \exp\left(-\tilde{D}_i n^2 \pi^2 t/R^{2-\omega}\right) - \exp(-D_o \beta_m^2 t)}{D_o \beta_m^2 - \tilde{D}_i n^2 \pi^2 / R^{2-\omega}} \right]. \quad (6)$$

III. STATISTICAL ANALYSIS

In this section, we use statistical analysis to study the impact of the PMP radius R on $r(t; R)$, where we write $r(t; R)$ instead of $r(t)$ to emphasize the dependence of $r(t)$ on R . In this way, we address two important sources of uncertainty regarding R that can arise in practice; (i) the variability of R across different PMPs within the same BNC fleece, (ii) variations in R across different BNC fleeces. Since R is one of the potential design parameters, the results presented in this section constitute a step towards understanding the possibilities and limits of tuning the considered CDD system by adjusting the PMP size.

A. PMP Size Distribution in one BNC fleece

In practice, the formation of the PMPs is a random process and, hence, not all PMPs in one BNC fleece have the same radius, i.e., R can be different for every PMP. Furthermore, the amount of drug molecules encapsulated in a PMP during its synthesis may depend on the PMP's size. However, to the best of our knowledge, no data in this regard is available.

¹In the proposed model, the total drug concentration is normalized to 1, since, similar to (1), we study the *relative* drug release.

Hence, in this paper, we consider two different hypotheses; namely, that the amount of drug molecules enclosed in a PMP is (i) *independent* of the PMP's size, (ii) *proportional to the volume* of the PMP. The drug release under Hypothesis (i) is studied analytically in this section, while (ii) is evaluated using Monte-Carlo simulations. Numerical results presented in Section IV show that for realistic PMP size distributions, the drug release under both hypotheses is almost identical.

To account for different PMP sizes, R is in the following modeled as a continuous, non-negative random variable with probability density function (pdf) $f_R(x)$. Under Hypothesis (i) the total drug release into the release medium in the presence of different sized PMPs can be expressed as $\mathbb{E}\{r(t; R)\}$, where $\mathbb{E}\{\cdot\}$ denotes the expectation operator with respect to $f_R(x)$. Furthermore, since $r(t)$ is a nonlinear function of R , in general,

$$\mu_r(t) = \mathbb{E}\{r(t; R)\} \neq r(t; \mathbb{E}\{R\}). \quad (7)$$

The true distribution of R is unknown and depends on the stochastic synthesis process of the PMPs. However, for a specific realization of this process, empirical data on the true distribution of R is available [13]. In order to obtain an *analytical model* for the distribution of R , we start from the hypothesis that the rate parameters of the exponential distributions in (4) are distributed according to the Gamma distribution with shape and rate parameters γ_n and ζ_n , respectively, i.e.,

$$\tilde{D}_i \alpha_n^2 \sim \text{Gamma}(\gamma_n, \zeta_n). \quad (8)$$

The Gamma distribution is a commonly used prior for the rate parameter of the exponential distribution [19]. In order to match (8) to the moments of R that can be experimentally observed, we establish the following theorem.

Theorem 1: Let $\tilde{D}_i \alpha_n^2 \sim \text{Gamma}(\gamma_n, \zeta_n)$. Then,

$$\mathbb{E}\{R\} = \mu_R = \frac{\Gamma(\gamma - 1/(2 - \omega))}{\Gamma(\gamma)} \zeta^{1/(2 - \omega)}, \quad (9)$$

$$\mathbb{E}\{R^2\} = \sigma_R^2 + \mu_R^2 = \frac{\Gamma(\gamma - 2/(2 - \omega))}{\Gamma(\gamma)} \zeta^{2/(2 - \omega)}, \quad (10)$$

where $\zeta = D_i n^2 \pi^2 \zeta_n$ and $\gamma = \gamma_n$ are independent of n , and σ_R^2 and $\Gamma(\cdot)$ denote the variance of R and the Gamma function, respectively.

Proof: Please see Appendix A. ■

The following corollary of Theorem 1 allows us to choose γ_n and ζ_n in (8) according to the experimentally observed statistics of R .

Corollary 1: From the first and second central moments of R , μ_R and σ_R^2 , γ and ζ are obtained from (9) and (10) as the solutions to the following system of equations:

$$\left[\frac{\mu_R \Gamma(\gamma)}{\Gamma(\gamma - 1/(2 - \omega))} \right]^{(2 - \omega)} - \zeta = 0, \quad (11)$$

$$\Gamma(\gamma) \frac{\Gamma(\gamma - 2/(2 - \omega))}{\Gamma(\gamma - 1/(2 - \omega))^2} - \left(1 + \frac{\sigma_R^2}{\mu_R^2} \right) = 0. \quad (12)$$

We confirm that the statistical model for the PMP sizes proposed in this paper is indeed accurate by comparing it to the experimentally observed particle size distribution from [13]. To this end, we set $\mu_R = 1 \mu\text{m}$ and $\sigma_R = 0.12 \mu\text{m}$ in

TABLE I
PARAMETER SIZE DISTRIBUTION

$K_{\text{LD}}(p q)$	This paper (8)	$\mathcal{N}(\mu_R, \sigma_R)$
Experiment [13]	$2.80 \cdot 10^{-2}$	$2.85 \cdot 10^{-2}$

agreement with [13] (data set EL10). To assess the quality of the fit, 10^8 random samples are drawn according to (8) and, as reference, from a Gaussian distribution, $\mathcal{N}(\mu_R, \sigma_R^2)$, with mean μ_R and variance σ_R^2 , respectively. Table I shows the agreement of both models with the experimental data in terms of their respective Kullback-Leibler divergences, where the Kullback-Leibler divergence between probability mass vectors $p = [p_1, \dots, p_N]$ and $q = [q_1, \dots, q_N]$ is defined as $K_{\text{LD}}(p||q) = \sum_{i=1}^N p_i \log(p_i/q_i)$, where $\log(\cdot)$ denotes the natural logarithm. Here, p and q correspond to the normalized empirical frequencies of the data and the random samples, respectively, after binning both in bins of width $0.14 \mu\text{m}$ as in [13]. As can be observed from Table I, both considered models are accurate, but (8) provides a even slightly better fit of the PMP size distribution than the Gaussian benchmark model.

Now that the analytical model for R in (8) is confirmed, $\mathbb{E}\{r(t; R)\}$ can be characterized as follows.

Theorem 2: Let $\tilde{D}_i \alpha_n^2 \sim \text{Gamma}(\gamma_n, \zeta_n)$. Then,

$$\mu_r(t) = 1 - \frac{6}{\pi^2} \sum_{n=1}^{\infty} \frac{1}{n^2} \left[\left(\frac{\zeta}{\zeta + \tilde{D}_i n^2 \pi^2 t} \right)^\gamma + 8 \sum_{m=1}^{\infty} \frac{\gamma \zeta^\gamma \tilde{D}_i n^2}{(2m-1)^2} \int_0^t \frac{\exp(-D_o \beta_m^2 (t - \tau))}{\left(\zeta + \tilde{D}_i n^2 \pi^2 \tau \right)^{(\gamma+1)}} d\tau \right]. \quad (13)$$

Proof: Please see Appendix B. ■

Theorem 2 is utilized in Section IV to show that for realistic values of μ_R and σ_R , $\mu_r(t) \approx r(t; \mu_R)$, i.e., that PMPs of the same size can be assumed if only one single BNC fleece is considered.

B. PMP Size Variations Across Different BNC Fleeces

Exploiting the results obtained in the previous section, we will now focus on the variability of $r(t; R)$ due to different PMP synthesis conditions in different BNC fleeces. To this end, we assume that the PMPs in each fleece have equal size, but the sizes of the PMPs in different fleeces vary from fleece to fleece. Hence, we consider R an unknown parameter for which only statistical knowledge is available. Specifically, we are interested in computing the variance of $r(t; R)$, $\sigma_r^2(t)$. Similar as in the previous section, we assume that the rate parameters of the exponential functions in (4) are distributed according to (8) and obtain the following result.

Theorem 3: Let $\tilde{D}_i \alpha_n^2 \sim \text{Gamma}(\gamma_n, \zeta_n)$. Then,

$$\sigma_r^2(t) = \sum_{n,l=1}^{\infty} a_n a_l \mathcal{A}_{n,l}(t) + 2 \sum_{n,m,l=1}^{\infty} b_{n,m,l} \mathcal{B}_{n,m,l}(t) + \sum_{n,m,l,k=1}^{\infty} c_{n,m,l,k} \mathcal{C}_{n,m,l,k}(t) - [1 - \mu_r(t)]^2, \quad (14)$$

TABLE II
DEFAULT PARAMETER VALUES [13]

Parameter	Default Value	Parameter	Default Value
a	3.54 mm	μ_R	1 μm
ω	0	σ_R	0.12 μm

where $a_n = 6/(\pi^2 n^2)$, $b_{n,m,l} = 8a_n a_l / [\pi^2 (2m-1)^2]$,
 $c_{n,m,l,k} = b_{n,m,l} b_{n,k,l} / (a_n a_l)$,

$$\mathcal{A}_{n,l}(t) = \left[\frac{\zeta}{\zeta + \tilde{D}_i \pi^2 (n^2 + l^2) t} \right]^\gamma, \quad (15)$$

$$\mathcal{B}_{n,m,l}(t) = \gamma \zeta^\gamma \tilde{D}_i n^2 \pi^2 \int_0^t \exp(-D_o \beta_m^2 (t-\tau)) / \left(\zeta + \tilde{D}_i \pi^2 (n^2 \tau + l^2 t) \right)^{(\gamma+1)} d\tau, \quad (16)$$

$$\mathcal{C}_{n,m,l,k}(t) = \gamma(\gamma+1) \zeta^\gamma \tilde{D}_i^2 n^2 l^2 \pi^4 \int_0^t \int_0^\theta \mathcal{D}_{n,m,l,k}(t, \tau, \theta) + \mathcal{D}_{l,k,n,m}(t, \tau, \theta) d\tau d\theta, \quad (17)$$

and

$$\mathcal{D}_{n,m,l,k}(t, \tau, \theta) = \exp(-D_o(\beta_m^2(\theta-\tau) + \beta_k^2\theta)) / \left(\zeta + \tilde{D}_i \pi^2 (n^2(t+\tau-\theta) + l^2(t-\theta)) \right)^{(\gamma+2)}. \quad (18)$$

Proof: Please see Appendix C. ■

Although the computation of $\sigma_r^2(t)$ involves the numerical evaluation of integrals, these integrals are definite integrals over finite intervals and can be computed efficiently using Gaussian quadrature.

IV. NUMERICAL RESULTS

In this section, numerical results for the analysis conducted in the previous section are presented and validated with experimental data and stochastic simulations. Unless otherwise noted, the default parameter values listed in Table II are used in agreement with experimental data in [13]. The free parameters D_i and D_o are set via exhaustive search to minimize the least-squares error between the analytical model and the experimental data. As a goodness-of-fit measure, we report the mean squared error (MSE) between model and data instead of the commonly used R^2 value, since the R^2 value is not meaningful for nonlinear regression as considered in this paper [20].

A. Drug Release from One BNC Fleece

First, we exploit data from experiments in which the CBD molecules are *not* embedded into PMPs, but released from a propylene glycol solution in the BNC fleece [13] to verify the proposed channel model (5) in isolation. In the considered scenario, the CBD molecules are released instantaneously in the BNC fleece, hence, the measured CBD concentration at the Rx corresponds to the channel impulse response in (5). Fig. 2 shows $h(t)$ for $D_o = 7.3 \cdot 10^{-2} \text{ mm}^2 \text{ h}^{-1}$ along with the experimental data and we observe that the agreement is excellent ($\text{MSE} = 1.6 \cdot 10^{-3}$).

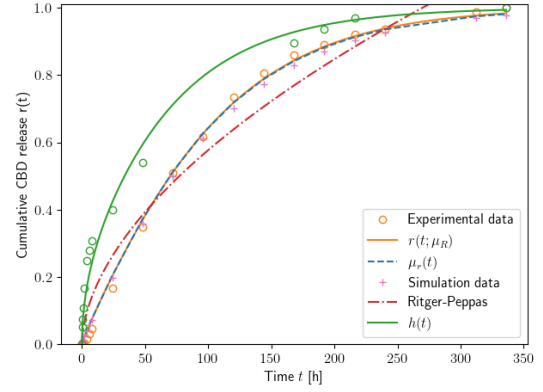


Fig. 2. CBD release from BNC fleece with (orange) and without (green) PMPs. Circle and cross markers denote experimental data from [13] (orange: data set EL10, green: data set propylene glycol) and simulation results, respectively.

Next, we consider the regular case, when the CBD molecules are released from PMPs inside the BNC fleece. Fig. 2 shows experimental data for this case along with $\mu_r(t)$, $r(t; \mu_R)$, and results from Monte-Carlo simulations, where, in the analytical and simulation results, $D_i = 1.62 \cdot 10^{-9} \text{ mm}^2 \text{ h}^{-1}$ and $D_o = 8.13 \cdot 10^{-2} \text{ mm}^2 \text{ h}^{-1}$. The Monte-Carlo simulations are performed by drawing 10^4 random samples according to (8) and then averaging (6) over these samples. In the simulations, it is assumed that the amount of CBD released from each PMP is proportional to its volume. We observe from Fig. 2 that the agreement between $r(t; \mu_R)$ and the experimental data is excellent ($\text{MSE} = 3.1 \cdot 10^{-4}$). Furthermore, we observe that the deviation between $\mu_r(t)$, $r(t; \mu_R)$, and the Monte-Carlo simulations is negligible. This latter observation has two important consequences. First, the agreement between Monte-Carlo simulations and $\mu_r(t)$ confirms that, for the considered PMP radius distribution, the assumption that all PMPs release the same total amount of CBD needed for our analysis is not critical, cf. Section III-A. Second, for the given PMP size statistics, since $\mu_r(t) \approx r(t; \mu_R)$, we can safely assume that all PMPs inside the same BNC fleece have the same size. Fig. 2 shows also that the proposed model significantly outperforms the Ritger-Peppas model (1), which yields $\text{MSE} = 5.2 \cdot 10^{-3}$, although both models involve two fitting parameters.

B. Unknown PMP Sizes Across Different BNC Fleeces

Finally, we study the impact of the correlation between R and D_i as expressed in (3) on $r(t; R)$ assuming that R is fixed, but we do not know its true value. To this end, we exploit Theorems 2 and 3 and compute $\sigma_r(t)$ as a measure of the uncertainty about $r(t; R)$ that results from knowing R only statistically. In practice, $\sigma_r(t)$ corresponds to the intrinsic variability in the drug releases from different BNC fleeces and is therefore an important parameter to consider for system design. To reflect the higher variability of PMP radii across different BNC fleeces as compared to the PMP size variation within one fleece, we assume a slightly larger $\sigma_R = 0.24 \mu\text{m}$ here than in the previous section.

Fig. 3 shows $\sigma_r(t')$ as a function of ω at time $t' = 24 \text{ h}$ for different values of D_i , i.e., for each ω , \tilde{D}_i in (3) is adjusted

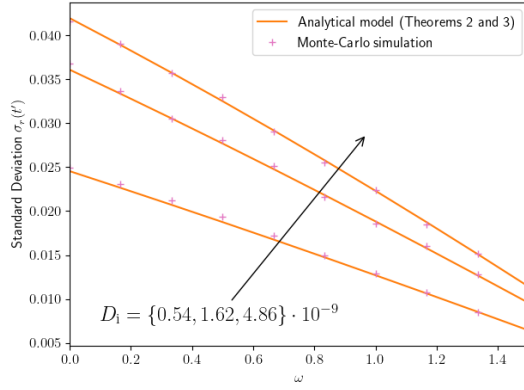


Fig. 3. $\sigma_r(t')$ as a function of ω at $t' = 24$ h as obtained from Theorems 2 and 3 (lines) and from Monte-Carlo simulations (markers), respectively, for different values of D_i .

such that D_i is the same for all values of ω . In this way, $r(t')$ is the same for all considered values of ω . We observe from Fig. 3 that ω does indeed have a significant impact on the variability of the drug release. Specifically, $\sigma_r(t')$ decreases as ω increases. Hence, the stronger R and D_i are correlated, the more deterministic is $r(t')$. Furthermore, we observe from Fig. 3 that this effect is more pronounced for large values of D_i . When $\omega \approx 0$, large values of D_i incur large values of $\sigma_r(t')$, while $\sigma_r(t')$ is comparatively small for small values of D_i . As ω increases, the difference between the $\sigma_r(t')$ for different values of D_i is reduced. Hence, when R and D_i are weakly correlated, the drug release is more sensitive towards variations in the PMP radius when the drug mobility inside the PMPs is large, while for strongly correlated R and D_i the sensitivity of the drug release to variations in the PMP radius is similar for different drug mobilities. From this observation, we conclude that more control over the PMP radius is required to ensure deterministic drug release for drug/PMP constellations for which ω is small as compared to ones for which ω is large.

V. CONCLUSION

In this paper, we have proposed a novel model for microparticle-based CDD from BNC. The proposed model has been validated with experimental data and shows excellent agreement while keeping the dimension of the parameter space low. Furthermore, a comprehensive statistical analysis has been presented that allows the characterization of the impact of the microparticle radius on the drug release. The presented results reveal that the sensitivity of the drug release with respect to changes of the particle radius depends on the degree to which particle radius and particle morphology are correlated.

To gain further insights on which specific drug/microparticle combinations can support particular drug release profiles, the values of ω corresponding to these combinations need to be characterized in future work. Such a characterization together with the results presented in this paper will guide the development of more and more refined microparticle-based CDD systems for specific applications that require high-precision control and reproducibility of drug release profiles.

A. Proof of Theorem 1

To simplify the notation, let $\tilde{\omega} = 2 - \omega$. Then, since $\tilde{D}_i \alpha_n^2 = \tilde{D}_i n^2 \pi^2 / R^{\tilde{\omega}} \sim \text{Gamma}(\gamma_n, \zeta_n)$, it follows from the scaling property of the Gamma distribution that $R^{-\tilde{\omega}} \sim \text{Gamma}(\gamma_n, \tilde{D}_i n^2 \pi^2 \zeta_n)$. Since this holds for any n , $R^{-\tilde{\omega}} \sim \text{Gamma}(\gamma, \zeta)$. Furthermore, by definition of the inverse Gamma distribution, we have $R^{\tilde{\omega}} \sim \text{InvGamma}(\gamma, \zeta)$, where $\text{InvGamma}(\alpha, \beta)$ denotes the inverse Gamma distribution with shape and rate parameters α and β , respectively. Now, according to the transformation theorem for random variables (RVs), the pdf of R , $f_R(x)$, is obtained from the pdf of $R^{\tilde{\omega}}$, $f_{R^{\tilde{\omega}}}(x)$, as follows

$$f_R(x) = f_{R^{\tilde{\omega}}}(x^{\tilde{\omega}}) \frac{dx^{\tilde{\omega}}}{dx} = \frac{\tilde{\omega} \zeta^\gamma}{\Gamma(\gamma)} x^{-(\tilde{\omega}\gamma+1)} \exp\left(-\frac{\zeta}{x^{\tilde{\omega}}}\right), \quad (19)$$

where we have substituted the pdf of the inverse Gamma distribution for $f_{R^{\tilde{\omega}}}(x)$.

The following computations yield $\mathbb{E}\{R\}$ and $\mathbb{E}\{R^2\}$ as required by the theorem.

$$\begin{aligned} \mathbb{E}\{R\} &= \frac{\tilde{\omega} \zeta^\gamma}{\Gamma(\gamma)} \int_0^\infty x^{-\tilde{\omega}\gamma} \exp\left(-\frac{\zeta}{x^{\tilde{\omega}}}\right) dx \\ &= \frac{\zeta^\gamma}{\Gamma(\gamma)} \int_0^\infty u^{-\gamma} \exp\left(-\frac{\zeta}{u}\right) u^{(1/\tilde{\omega})-1} du \\ &= \frac{\zeta^\gamma}{\Gamma(\gamma)} \int_0^\infty u^{-[\gamma-(1/\tilde{\omega})+1]} \exp\left(-\frac{\zeta}{u}\right) du \\ &= \frac{\Gamma(\gamma - 1/\tilde{\omega})}{\Gamma(\gamma)} \frac{\zeta^\gamma}{\zeta^{\gamma-1/\tilde{\omega}}} = \frac{\Gamma(\gamma - 1/\tilde{\omega})}{\Gamma(\gamma)} \zeta^{1/\tilde{\omega}}, \quad (20) \end{aligned}$$

$$\begin{aligned} \mathbb{E}\{R^2\} &= \frac{\tilde{\omega} \zeta^\gamma}{\Gamma(\gamma)} \int_0^\infty x^{-2\tilde{\omega}\gamma+1} \exp\left(-\frac{\zeta}{x^{\tilde{\omega}}}\right) dx \\ &= \frac{\zeta^\gamma}{\Gamma(\gamma)} \int_0^\infty u^{-\gamma+1/\tilde{\omega}} \exp\left(-\frac{\zeta}{u}\right) u^{(1/\tilde{\omega})-1} du \\ &= \frac{\zeta^\gamma}{\Gamma(\gamma)} \int_0^\infty u^{-[\gamma-(2/\tilde{\omega})+1]} \exp\left(-\frac{\zeta}{u}\right) du \\ &= \frac{\Gamma(\gamma - 2/\tilde{\omega})}{\Gamma(\gamma)} \frac{\zeta^\gamma}{\zeta^{\gamma-2/\tilde{\omega}}} = \frac{\Gamma(\gamma - 2/\tilde{\omega})}{\Gamma(\gamma)} \zeta^{2/\tilde{\omega}}, \quad (21) \end{aligned}$$

where we used the substitution $u = x^{\tilde{\omega}}$ in both equations. Substituting the definition of $\tilde{\omega}$ into (20), (21), Theorem 1 follows. This completes the proof.

B. Proof of Theorem 2

In order to compute $\mathbb{E}\{r(t; R)\}$, we exploit $\tilde{D}_i \alpha_n^2 \sim \text{Gamma}(\gamma, \zeta_n)$, cf. Theorem 1, and compute the expectations

of the summands in (6) separately. We obtain

$$\begin{aligned}
& \mathbb{E} \left\{ \exp \left(-\tilde{D}_i \alpha_n^2 t \right) \right\} \\
&= \frac{\zeta_n^\gamma}{\Gamma(\gamma)} \int_0^\infty \exp(-tx) x^{\gamma-1} \exp(-\zeta_n x) dx \\
&= \frac{\zeta_n^\gamma}{\Gamma(\gamma)} \int_0^\infty x^{\gamma-1} \exp(-(\zeta_n + t)x) dx \\
&= \frac{\zeta_n^\gamma}{(\zeta_n + 1)^\gamma} = \left(\frac{\zeta}{\zeta + \tilde{D}_i n^2 \pi^2 t} \right)^\gamma, \quad (22)
\end{aligned}$$

and,

$$\begin{aligned}
& \mathbb{E} \left\{ \frac{\tilde{D}_i \alpha_n^2 \exp(-\tilde{D}_i \alpha_n^2 t) - \exp(-D_o \beta_m^2 t)}{D_o \beta_m^2 - \tilde{D}_i \alpha_n^2} \right\} \\
&= \frac{\zeta_n^\gamma}{\Gamma(\gamma)} \int_0^\infty \frac{\exp(-xt) - \exp(-D_o \beta_m^2 t)}{D_o \beta_m^2 - x} x^\gamma \exp(-\zeta_n x) dx \\
&= \frac{\zeta_n^\gamma}{\Gamma(\gamma)} \int_0^\infty \frac{\exp(-(\zeta_n + t)x) - \exp(-D_o \beta_m^2 t - \zeta_n x)}{D_o \beta_m^2 - x} x^\gamma dx \\
&\stackrel{(a)}{=} \frac{\zeta_n^\gamma}{\Gamma(\gamma)} \int_0^\infty \int_0^t \exp(-(\tau + \zeta_n)x - D_o \beta_m^2 (t - \tau)) x^\gamma d\tau dx \\
&= \int_0^t \frac{\zeta_n^\gamma}{(\zeta_n + \tau)^{(\gamma+1)}} \exp(-D_o \beta_m^2 (t - \tau)) d\tau, \quad (23)
\end{aligned}$$

where we have utilized the fact that the fraction in the integrand on the left-hand side of (a) can be written in terms of a convolution in t and that the integrals on the right-hand side of (a) can be interchanged. Substituting the definition of ζ_n from Theorem 1 and collecting terms, Theorem 2 follows. This completes the proof.

C. Proof of Theorem 3

First, let us rewrite $r(t)$ as follows

$$r(t) = 1 - \sum_{n=1}^{\infty} a_n A_n(t) + \sum_{n,m=1}^{\infty} g_{n,m} G_{n,m}(t), \quad (24)$$

where $g_{n,m} = a_n 8\pi^2 / (2m-1)^2$, $A_n(t) = \exp(-\tilde{D}_i \alpha_n^2 t)$, and

$$G_{n,m}(t) = \frac{\tilde{D}_i \alpha_n^2 \exp(-\tilde{D}_i \alpha_n^2 t) - \exp(-D_o \beta_m^2 t)}{D_o \beta_m^2 - \tilde{D}_i \alpha_n^2}. \quad (25)$$

Then,

$$\begin{aligned}
\sigma_r^2(t) &= \mathbb{E} \{ r(t)^2 \} - \mu_r(t)^2 \\
&= \mathbb{E} \left\{ \left[\sum_{n=1}^{\infty} a_n A_n(t) + \sum_{n,m=1}^{\infty} g_{n,m} G_{n,m}(t) \right]^2 \right\} + 1 \\
&\quad - 2 \mathbb{E} \left\{ \sum_{n=1}^{\infty} a_n A_n(t) + \sum_{n,m=1}^{\infty} g_{n,m} G_{n,m}(t) \right\} - \mu_r(t)^2 \\
&= \mathbb{E} \left\{ \left[\sum_{n=1}^{\infty} a_n A_n(t) + \sum_{n,m=1}^{\infty} g_{n,m} G_{n,m}(t) \right]^2 \right\} + 1 \\
&\quad - 2 [1 - \mu_r(t)] - \mu_r(t)^2 \\
&= \mathbb{E} \left\{ \left[\sum_{n=1}^{\infty} a_n A_n(t) + \sum_{n,m=1}^{\infty} g_{n,m} G_{n,m}(t) \right]^2 \right\} \\
&\quad - [1 - \mu_r(t)]^2. \quad (26)
\end{aligned}$$

Hence, in order to compute $\sigma_r(t)^2$, after opening the square in the expectation on the right-hand side of (26), the following terms need to be computed:

$$\mathbb{E} \{ A_n(t) A_l(t) \}, \quad (27)$$

$$\mathbb{E} \{ A_n(t) G_{l,k}(t) \}, \quad (28)$$

$$\mathbb{E} \{ G_{n,m}(t) G_{l,k}(t) \}, \quad (29)$$

where l, k are positive integers. From the proof of Theorem 1, we recall that $R^{-(2-\omega)} \sim \text{Gamma}(\gamma, \zeta)$. Hence, substituting the pdf of the Gamma distribution in (27), we obtain

$$\begin{aligned}
& \mathbb{E} \{ A_n(t) A_l(t) \} \\
&= \frac{\zeta^\gamma}{\Gamma(\gamma)} \int_0^\infty \exp(-\tilde{D}_i (n^2 + l^2) \pi^2 t x) x^{\gamma-1} \exp(-\zeta x) dx \\
&= \left[\frac{\zeta}{\zeta + \tilde{D}_i \pi^2 (n^2 + l^2) t} \right]^\gamma. \quad (30)
\end{aligned}$$

Before we proceed to computing (28) and (29), we require some more notation. In particular, for any square-integrable function $f(t)$, let its *Fourier transform* $\hat{f}(\xi)$ be defined as

$$\hat{f}(\xi) = \mathbb{F} [f(t)] = \int_{-\infty}^{\infty} f(t) \exp(-j\xi t) dt, \quad (31)$$

where j denotes the imaginary unit. Similarly, let the *inverse Fourier transform* of a function $\hat{f}(\xi)$ be defined as follows

$$f(t) = \mathbb{F}^{-1} [\hat{f}(\xi)] = \frac{1}{2\pi} \int_{-\infty}^{\infty} \hat{f}(\xi) \exp(j\xi t) d\xi. \quad (32)$$

With these definitions, we obtain

$$\begin{aligned} \mathbb{F}[A_n(t)G_{l,k}(t)] &= \frac{\tilde{D}_i\alpha_n^2}{D_o\beta_m^2 - \tilde{D}_i\alpha_n^2} \\ &\cdot \left[\frac{1}{\tilde{D}_i(\alpha_n^2 + \alpha_l^2) + j\xi} - \frac{1}{D_o\beta_m^2 + \tilde{D}_i\alpha_l^2 + j\xi} \right], \\ &= \frac{\tilde{D}_i\alpha_n^2}{\left[\tilde{D}_i(\alpha_n^2 + \alpha_l^2) + j\xi \right] \left(D_o\beta_m^2 + \tilde{D}_i\alpha_l^2 + j\xi \right)}, \end{aligned} \quad (33)$$

where we have exploited repeatedly that $t \geq 0$ and $\mathbb{F}[\exp(-ct)u(t)] = 1/(c + j\xi)$, where $c > 0$ is any positive constant and $u(t)$ denotes the unit step function. Since multiplication in the Fourier domain corresponds to convolution in the time domain, we obtain

$$\begin{aligned} \mathbb{E}\{A_n(t)G_{l,k}(t)\} &= \mathbb{E}\{\mathbb{F}^{-1}[\mathbb{F}[A_n(t)G_{l,k}(t)]]\} \\ &= \mathbb{E}\left\{ \tilde{D}_i\alpha_n^2 \int_0^t \exp(-\tilde{D}_i(\alpha_n^2 + \alpha_l^2)\tau) \right. \\ &\quad \cdot \exp\left(-\left(D_o\beta_m^2 + \tilde{D}_i\alpha_l^2\right)(t - \tau)\right) d\tau \left. \right\} \\ &= \mathbb{E}\left\{ \tilde{D}_i n^2 \pi^2 R^{-(2-\omega)} \int_0^t \exp(-D_o\beta_m^2(t - \tau)) \right. \\ &\quad \cdot \exp\left(-\tilde{D}_i\pi^2(n^2\tau + l^2t)R^{-(2-\omega)}\right) d\tau \left. \right\}. \end{aligned} \quad (34)$$

Substituting the pdf of the Gamma distribution in (34), we proceed by exchanging integrals as in the second part of the proof of Theorem 2 and obtain after some straightforward computations

$$\begin{aligned} \mathbb{E}\{A_n(t)G_{l,k}(t)\} &= \gamma \tilde{D}_i n^2 \pi^2 \zeta^\gamma \int_0^t \frac{\exp(-D_o\beta_m^2(t - \tau))}{\left[\zeta + \tilde{D}_i\pi^2(n^2\tau + l^2t)\right]^{\gamma+1}} d\tau. \end{aligned} \quad (35)$$

The computation of (29) follows the same strategy. After some simplification in the Fourier domain, $\mathbb{F}[G_{n,m}(t)G_{l,k}(t)]$ is obtained as shown in (36) on the next page. Applying the inverse Fourier transform to (36), exploiting again that multiplication in the Fourier domain corresponds to convolution in the time domain, and substituting the pdf of the Gamma function in (29) finally yields (37) as shown on the next page.

Collecting terms from (30), (35), (37), and substituting in (26), Theorem 3 follows immediately. This completes the proof.

REFERENCES

- [1] I. F. Akyildiz, M. Pierobon, S. Balasubramaniam, and Y. Koucheryavy, "The internet of Bio-Nano things," *IEEE Commun. Mag.*, vol. 53, no. 3, pp. 32–40, Mar. 2015.
- [2] L. Felicetti, M. Femminella, G. Reali, and P. Liò, "Applications of molecular communications to medicine: A survey," *Nano Commun. Netw.*, vol. 7, pp. 27–45, Mar. 2016.
- [3] U. A. K. Chude-Onkonkwo, R. Malekian, B. T. Maharaj, and A. V. Vasilakos, "Molecular communication and nanonetwork for targeted drug delivery: A survey," *IEEE Commun. Surv. Tut.*, vol. 19, no. 4, pp. 3046–3096, Fourthquarter 2017.
- [4] Q. Zhao, M. Li, and L. Lin, "Release rate optimization in molecular communication for local nanomachine-based targeted drug delivery," *IEEE Trans. NanoBiosci.*, vol. 20, no. 4, pp. 396–405, Oct. 2021.
- [5] A. K. Shrivastava, D. Das, R. Mahapatra, and S. P. Mohanty, "dmole: A novel transceiver for mobile molecular communication using robust differential detection techniques," *IEEE Trans. NanoBiosci.*, vol. 19, no. 4, pp. 609–621, Oct. 2020.
- [6] H. K. Rudsari, M. Veletić, J. Bergsland, and I. Balasingham, "Targeted drug delivery for cardiovascular disease: Modeling of modulated extracellular vesicle release rates," *IEEE Trans. NanoBiosci.*, vol. 20, no. 4, pp. 444–454, Oct. 2021.
- [7] M. Schäfer *et al.*, "Channel responses for the molecule release from spherical homogeneous matrix carriers," *IEEE Trans. Mol. Biol. Multi-Scale Commun.*, vol. 8, no. 4, pp. 212–228, Dec. 2022.
- [8] P. L. Ritger and N. A. Peppas, "A simple equation for description of solute release i. Fickian and non-fickian release from non-swollable devices in the form of slabs, spheres, cylinders or discs," *J. Controlled Release*, vol. 5, no. 1, pp. 23–36, Jun. 1987.
- [9] L. Pourtalebi Jahromi, M. Ghazali, H. Ashrafi, and A. Azadi, "A comparison of models for the analysis of the kinetics of drug release from PLGA-based nanoparticles," *Heliyon*, vol. 6, no. 2, Feb. 2020.
- [10] Y. Pöttinger, D. Kralisch, and D. Fischer, "Bacterial nanocellulose: the future of controlled drug delivery?" *Therapeutic Delivery*, vol. 8, no. 9, pp. 753–761, Aug. 2017.
- [11] M. Iguchi, S. Yamanaka, and A. Budhiono, "Bacterial cellulose—a masterpiece of nature's arts," *J. Mater. Sci.*, vol. 35, no. 2, pp. 261–270, Jan. 2000.
- [12] S. Kalia and L. Avérous, *Biopolymers: Biomedical and Environmental Applications*. John Wiley & Sons, 2011, vol. 70.
- [13] T. Bellmann, J. Thamm, U. Beekmann, D. Kralisch, and D. Fischer, "In situ formation of polymer microparticles in bacterial nanocellulose using alternative and sustainable solvents to incorporate lipophilic drugs," *Pharmaceutics*, vol. 15(2), no. 559, Feb. 2023.
- [14] J. Siepmann, K. Elkharraz, F. Siepmann, and D. Klose, "How autocatalysis accelerates drug release from PLGA-based microparticles: A quantitative treatment," *Biomacromol.*, vol. 6, no. 4, pp. 2312–2319, Jul. 2005.
- [15] D. Klose, F. Siepmann, K. Elkharraz, and J. Siepmann, "PLGA-based drug delivery systems: Importance of the type of drug and device geometry," *Int. J. Pharmaceutics*, vol. 354, no. 1, pp. 95–103, Apr. 2008.
- [16] T. Casalini *et al.*, "Mathematical modeling of PLGA microparticles: From polymer degradation to drug release," *Mol. Pharmaceutics*, vol. 11, no. 11, pp. 4036–4048, Nov. 2014.
- [17] J. Crank, *The Mathematics of Diffusion*. Oxford University Press, 1979.
- [18] V. Tangsatianpan, S. Torgbo, and P. Sukyai, "Release kinetic model and antimicrobial activity of freeze-dried curcumin-loaded bacterial nanocellulose composite," *Polymer Sci., Ser. A*, vol. 62, no. 3, pp. 218–227, Jun. 2020.
- [19] A. Gelman *et al.*, *Bayesian Data Analysis*. CRC Press, 2013.
- [20] A.-N. Spiess and N. Neumeyer, "An evaluation of R2 as an inadequate measure for nonlinear models in pharmacological and biochemical research: A Monte Carlo approach," *BMC Pharmacol.*, vol. 10, no. 1, p. 6, Jun. 2010.

$$\mathbb{F}[G_{n,m}(t)G_{l,k}(t)] = \tilde{D}_i^2 \alpha_n^2 \alpha_l^2 \left\{ \frac{1}{\left[\tilde{D}_i(\alpha_n^2 + \alpha_l^2) + j\xi \right] \left(\tilde{D}_i \alpha_n^2 + D_o \beta_k^2 + j\xi \right) [D_o(\beta_m^2 + \beta_k^2) + j\xi]} + \frac{1}{\left[\tilde{D}_i(\alpha_n^2 + \alpha_l^2) + j\xi \right] \left(D_o \beta_m^2 + \tilde{D}_i \alpha_l^2 + j\xi \right) [D_o(\beta_m^2 + \beta_k^2) + j\xi]} \right\} \quad (36)$$

$$\mathbb{E}\{G_{n,m}(t)G_{l,k}(t)\} = \tilde{D}_i^2 (n^2 + l^2) \pi^4 \zeta^\gamma \alpha (\alpha + 1) \int_0^t \int_0^\theta \left[\frac{\exp(-D_o(\beta_m^2(\theta - \tau) + \beta_k^2 \theta))}{\left[\zeta + \tilde{D}_i \pi^2 (n^2(t + \tau - \theta) + l^2(t - \theta)) \right]^{\gamma+2}} + \frac{\exp(-D_o(\beta_k^2(\theta - \tau) + \beta_m^2 \theta))}{\left[\zeta + \tilde{D}_i \pi^2 (l^2(t + \tau - \theta) + n^2(t - \theta)) \right]^{\gamma+2}} \right] d\tau d\theta \quad (37)$$
